NOMA-aided UAV communications over correlated Rician shadowed fading channels

Tan, Ernest Zheng Hui; Madhukumar, A. S.; Sirigina, Rajendra Prasad; Krishna, Anoop Kumar

2020

NOMA-aided UAV Communications over Correlated Rician Shadowed Fading Channels

Tan Zheng Hui Ernest, A S Madhukumar, Rajendra Prasad Sirigina, and Anoop Kumar Krishna

Abstract—In this paper, non-orthogonal multiple access (NOMA) is investigated as a viable solution to address spectrum scarcity in unmanned aerial vehicle (UAV) communications. Specifically, the performance analysis of a NOMA-aided UAV communication system (UCS) with dual-diversity receivers on UAVs is conducted over bivariate Rician shadowed fading channels. Using newly obtained closed-form expressions for the joint probability density function (PDF) and joint cumulative distribution function (CDF), the outage probability and finite signal-to-noise ratio (SNR) diversity gain of NOMA-aided UCS are investigated within a stochastic geometry framework. A comprehensive analysis reveals that NOMA-aided UCSs can support more UAVs on the same spectrum than OMA-based systems, with similar outage probability. It is also shown that the cross correlation affects the diversity gain of NOMA-aided and OMA-based UCSs only at low SNR regimes. Therefore, NOMA-aided UCSs can be an attractive alternative over OMA-based UCSs in future wireless systems.

Index Terms—Unmanned Aerial Vehicle, NOMA, Outage Probability, Finite signal-to-noise ratio (SNR), Diversity, Correlation, Bivariate Rician Shadowed Fading.

I. INTRODUCTION

A. Motivation

Unmanned aerial vehicles (UAVs) have received recent interest in providing next-generation wireless services. However, the popularity of UAV-based applications presents a challenge in terms of spectrum utilization. At the moment, the L-band and C-band, which have been allocated for UAV communications, concurrently supports other existing systems as well [1]. Thus, only a limited portion of the L-band and C-band can be utilized to support UAV communications. If left unchecked, UAV-aided wireless services may encounter performance degradations in future wireless systems as a result of spectrum scarcity [2].

Towards this end, one can consider non-orthogonal multiple access (NOMA), i.e., power-domain NOMA, as a means to address spectrum efficiency in UAV communications. As one of the key enabling technologies being considered for future wireless systems, NOMA can be employed to support more UAVs over orthogonal multiple access (OMA) schemes.

Tan Zheng Hui Ernest is with the School of Computer Science and Engineering, Nanyang Technological University, Singapore e-mail: (tanz0119@e.ntu.edu.sg).

A S Madhukumar is with the School of Computer Science and Engineering, Nanyang Technological University, Singapore e-mail: (asmadhukumar@ntu.edu.sg).

Rajendra Prasad Sirigina is with the School of Computer Science and Engineering, Nanyang Technological University, Singapore e-mail: (raje0015@ntu.edu.sg).

Anoop Kumar Krishna is with Airbus Singapore Pte Ltd, Singapore e-mail: (anoopkumar.krishna@airbus.com).

Specifically, in NOMA-aided UAV communication systems (UCSs), the ground station (GS) employs superposition coding to communicate with multiple downlink UAVs simultaneously. Subsequently, the downlink UAV with the strongest channel gain employs successive interference cancellation (SIC) to detect the desired signal [3]. On the other hand, downlink UAVs with weak channel gain employ interference-ignorant detection, i.e., treating other UAVs' messages as noise, for message detection [3].

B. Related Literature

As a result of substantial research interest, a plethora of works have investigated the reliability of downlink NOMA in terms of outage probability, e.g., [4]–[11]. However, the studies mentioned above have primarily focused on cellular systems. Thus, critical insights from these works cannot be fully applied for UCSs, owing to a difference in the environment and operating constraints between cellular and UAV communications, as shown in the rest of this section.

1) UAV Channel Models: One of the key differences between cellular and UAV communications is the channel model. To illustrate, outage probability analysis have been conducted for NOMA-aided cellular communications over Rayleigh fading channels [4], [5], [7], [10], [11], and Nakagami-m fading channels [8], while the work in [6] only considered large-scale fading in the channel model. Even for NOMA-aided UAV communications, the Rayleigh [12], [13] and Nakagami-m [9] fading models are commonly used in the literature. In contrast, apart from Rayleigh fading and Nakagami-m fading channels, UAV communications can also occur over Rician fading channels [1], [14]–[17], and Rician shadowed fading channels [15], [18].

The main characteristic separating the Rician fading channel from the Rician shadowed fading channel is that the line-of-sight (LOS) component undergoes shadowing in the latter [18]. In particular, the LOS and non-LOS (NLOS) components in Rician shadowed fading channels are modeled using the non-centered Chi-squared distribution. Additionally, shadowing experienced by the LOS component is modeled using the Nakagami-m distribution. Therefore, in Rician shadowed fading channel models, the relation between the ratio of the LOS-to-NLOS components and the degree of LOS shadowing is defined using the Rician K factor and Nakagami-m shaping parameter, respectively.

In the literature, such univariate fading models have been used as the basis of UAV channel models, e.g., [14] and [18], and are suitable for single-antenna receivers. However, dual-diversity receivers, i.e., dual-antenna receivers, may experience

correlation due to insufficient antenna separation, heading of the UAV, UAV elevation angle, and the received signal's angle of arrival [19]–[23]. Therefore, in such cases, dual-diversity receivers may experience bivariate Rician shadowed fading when transmissions occur over Rician shadowed fading channels. Thus far, multivariate and bivariate fading models have been investigated in diversity combining systems, e.g., in [24]–[26], and multi-antenna UAV communication systems [20]–[22], [27] to model the spatial correlation at the reception antennas. The study in [28] also followed similar analysis to investigate the effect of correlation in multi-antenna receivers for UAV communications. A bivariate Rician shadowed fading channel was modeled in [19] using a power series approach, with related performance analysis also conducted for a downlink NOMA-aided UCS with single-antenna receivers. However, investigations into the performance of NOMA-aided dual-diversity UCSs over bivariate Rician shadowed fading channels remain an open problem.

2) UAV Deployment Characteristics: Apart from channel modeling, the deployment of UAVs is another distinguishing feature in UCSs. With UAVs increasingly playing a multitude of roles, e.g., end-users [29] and aerial BSs [30]–[32], any effective analysis of UCSs must consider the deployment of UAVs. In this spirit, one can employ stochastic geometry as a useful tool to capture the essential characteristics of UAV deployment. For instance, modeling the spatial location of terrestrial nodes using a Poisson point process (PPP) is a widely used technique in the literature. Yet, various studies, i.e., [29], [30], [32], have noted the unsuitability of the PPP model for UCSs. Specifically, from a practical perspective, the PPP model becomes unsuitable when the number of deployed UAVs in the UCS is fixed [29], [30].

Instead, one can utilize the binomial point process (BPP) model to provide an accurate characterization of UAV deployment in UCSs [29], [30]. Under the BPP model, a fixed number of UAVs are uniformly distributed in a finite-sized cell [29], [30]. Modeling the spatial location of UAVs in UCSs using BPP have been noted in recent studies, e.g., [29]–[31], [33]. However, the BPP model has not been extensively utilized to analyze NOMA-aided UCSs.

3) Analysis of Finite SNR Diversity Gain: Finally, it is noted that existing NOMA-related studies have largely focused on outage probability, e.g., [10], [11], and throughput, e.g., [34], [35], as key performance metrics. To further complement the analysis, one can also analyze the finite signal-to-noise ratio (SNR) diversity gain of NOMA-aided systems. In the literature, finite SNR diversity gain has been used to evaluate the outage performance of wireless systems, e.g., in [14], [36]–[38]. In particular, finite SNR diversity gain is a measure of the outage probability slope at particular SNR levels [37]. Through the analysis of finite SNR diversity gain, the outage probability behaviors that are only observable at non-asymptotic SNR regimes, i.e., finite SNR regimes, are revealed. Such finite SNR analysis is particularly useful in providing an accurate picture of a system's outage performance since most wireless systems typically operate at low-to-moderate SNR ranges [38]. For instance, the SNR needed to achieve a particular rate of error decay, through turbo codes or low-density parity-

check codes, can be estimated via finite SNR analysis [36]. Finite SNR analysis can also be used to determine the upper and lower limits of bit error rate performance [39], [40], and also to determine scenarios that can lead to a wireless system becoming interference-limited [14], [38]. Yet, despite gaining research interest in recent years, e.g., [14], [38], [41], [42], only a few NOMA-related studies, e.g., [4], [8], have quantified the asymptotic diversity gain of NOMA-aided networks. Thus, to the best of our knowledge, the analysis of finite SNR diversity gain in NOMA-aided networks remains an open research problem.

C. Main Contributions

Despite several related studies on correlated UAV communications, e.g., [9], [12], [13], [28], the viability of NOMA-aided UCSs operating in realistic operating environments has not received much attention.

To this end, a comprehensive performance analysis of a NOMA-aided UCS, comprising selection combining dual-diversity receivers on UAVs, communicating over bivariate Rician shadowed fading channels is conducted in this paper. New closed-form expressions are obtained for the joint probability density function (PDF), and joint cumulative distribution function (CDF) of the bivariate Rician shadowed fading model through a power series approach.

While the joint PDF and joint CDF expressions for the bivariate Rician shadowed fading are already available in [26], usage of the exact expressions require numerical methods that may render certain types of performance analysis intractable. In contrast, this paper shows that the existing complicated expressions can be further simplified through power series manipulations. Thus, resulting in new joint PDF and CDF expressions that are easy to evaluate. The exact truncation error and truncation error upper bound are also presented for the new expressions based on the work in [43]. Compared to the truncation analysis in [43], which involves two infinite series, we demonstrate that the truncation analysis approach seen in [43] can be extended for two nested infinite series.

From the derived joint CDF expression, closed-form outage probability and finite SNR diversity gain expressions for NOMA-aided and OMA-based UCSs are presented within a stochastic geometry framework. An extensive analysis demonstrates that the NOMA-aided UCS can support a larger number of UAVs on the same spectrum than OMA-based systems while achieving highly similar outage probability. Furthermore, it is shown that cross correlation only affects the diversity gain of both NOMA and OMA transmissions at low SNR regimes.

D. Paper Organization

The organization of this paper is as follows. The system model of the NOMA-aided UCS is introduced in Section II, while the bivariate Rician shadowed fading model is presented In Section III. Thereafter, expressions for outage probability and finite SNR diversity gain are presented in Sections IV and V, respectively. Finally, the numerical results are discussed in Section VI before the conclusion of the paper in Section VII.
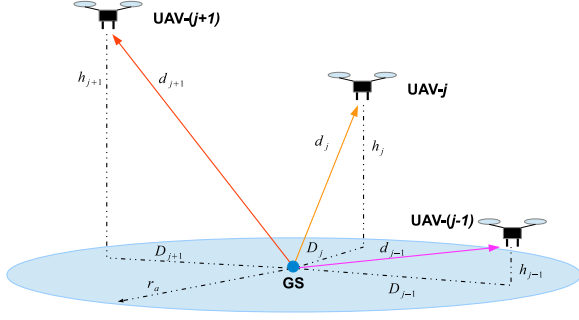
II. System Model

Fig. 1. An illustration of the NOMA-aided UCS operating in a suburban environment. The GS employs downlink NOMA to transmit data to the UAVs equipped with dual-diversity receivers, i.e., two reception antennas. At the UAVs, selection combining is employed to recover the transmitted data from the GS.

Consider a NOMA-aided UCS operating in a suburban environment, comprising one single-antenna GS and N_D downlink UAVs equipped with dual-diversity receivers (Fig. 1). [1] The GS in the NOMA-aided UCS employs downlink NOMA to transmit data, while selection combining is employed as the reception strategy at the N_D downlink UAVs. [2] However, due to insufficient spacing between the receive antennas at the UAVs and the relative position of the UAVs to the GS, the downlink NOMA transmissions are assumed to occur over correlated fading channels. Separately, based on studies in [29] and [30], a BPP model is employed in the present work to account for the spatial locations of the UAVs. It is also assumed that the UAVs are operating at a minimum altitude of h_{min} [29], [30], with compensated Doppler shifts [14]. [3] Furthermore, each UAV is assumed to be operating at different altitudes in order to consider various UAV deployment scenarios, e.g., high or low altitude platforms, in multi-tier UAV networks. Lastly, as a suburban setting is considered in this work, the bivariate Rician shadowed fading model is assumed for the UAV channels to account for the correlation between the receive antennas at the downlink UAVs, and also the small-scale Rician fading and LOS shadowing in the suburban environment [44], [45].
[4] [5]

---

[1]A practical realization of the NOMA-aided UCS can be accomplished with help from existing cellular infrastructure in suburban places due to the density of GSs, i.e., base stations.

[2]Discussions on suitable precoding/beamforming methods are beyond the scope of the current work and will be investigated in future extensions of this paper.

[3]In practice, UAV communications can occur on the L-band [1]. Under such circumstances, it has been shown that Doppler shifts is not an issue for civil aircraft, i.e., aeronautical communications, which operate at higher aircraft velocities than UAVs [38]. Therefore, for UAV communications, Doppler shifts can be compensated and is not the main performance limiting factor in UCSs.

[4]It is worth noting that the analytical approach in this paper is also extensible to multi-antenna selection combining receivers.

[5]The Rician K factor of each GS-to-UAV link in the present work is chosen based on the study in [1]. However, future extensions of this paper can look into modeling the Rician K factor based on UAV altitude and elevation angle using the approach in [46].

A. Distribution of UAV Spatial Locations

Let the spatial location of the UAVs follow a uniform distribution in a disc centered at origin O above the GS with radius r_a and angle $[0, 2\pi)$. Then, the Euclidean distance (km) between downlink UAV-j and the GS is $d_j = \sqrt{D_j^2 + h_j^2}$, where $1 \leq j \leq N_D$ is the index of downlink UAV-j, D_j is the projected Euclidean distance on the ground plane between the GS and downlink UAV-j, $h_j = h_{min} + \overline{\omega}\frac{j}{N_D}$ is the altitude of downlink UAV-j, $\overline{\omega} > 0$ is the altitude separation factor between the downlink UAVs.

As the spatial location of downlink UAV-j follows a uniform distribution, the PDF $f_{d_j}(w)$ of d_j is given as [29, eq. (3)], [33]:

$$f_{d_j}(w) = \frac{2w}{r_a^2}, \tag{1}$$

where $L_{m,j} \leq w \leq L_{p,j}$, $L_{m,j} = h_j$, and $L_{p,j} = \sqrt{h_j^2 + r_a^2}$. Using the PDF $f_{d_j}(w)$, one can analyze the performance of correlated downlink NOMA transmissions with the assumption of the UAV spatial distribution taken into consideration.

B. Instantaneous SINR at Downlink UAV-j

Following downlink NOMA transmission principles, the GS uses superposition coding to transmit the signal-of-interest (SOI) to all downlink UAVs. Specifically, a SIC detector is employed at downlink UAV-j to detect the SOI in the presence of multi-user interference (MUI) from the SOIs of the other downlink UAVs. Let $R_{j,l}$ be the instantaneous channel envelope of the lth receive antenna at downlink UAV-j for $l \in \{1, 2\}$, where $R_{j,l}$ follows a bivariate Rician shadowed distribution. Then, the instantaneous signal-to-interference-plus-noise ratio (SINR) of the lth receive antenna at downlink UAV-j $(SINR_{j,l})$ is:

$$SINR_{j,l} = \frac{P_r a_j d_j^{-L}|R_{j,l}|^2}{1 + P_r d_j^{-L}|R_{j,l}|^2 \sum_{i=1}^{j-1} a_i} \tag{2}$$

where $P_r \propto \frac{P_t}{P_L \eta}$ is the normalized average received power [38], P_t is the transmit power of the GS, $P_L = \left(\frac{4\pi \cdot 10^9}{3 \cdot 10^8} f_c\right)^2$ is the pathloss, L is the pathloss exponent, $\eta = -174 + 10\log_{10}(B_W)$ is the strength of the additive white Gaussian noise (AWGN) in dBm [47], f_c is the carrier frequency (MHz), B_W is the bandwidth (Hz), and a_j is the power allocation factor for DL UAV-j such that $\sum_{j=1}^{N_D} \alpha_j = 1$. [6]

III. Bivariate Rician Shadowed Fading Model

In UAV communications, correlation of the UAV channels can occur due to insufficient spacing between the UAV's receive antenna, UAV heading, and UAV position relative to the GS [19]–[22]. As such, we introduce the bivariate Rician shadowed fading model in this section to model the correlated UAV channels.

---

[6]The current work can be extended to consider multi-cell deployments by treating interfering UAVs as co-channel interference.

To begin, a pair of bivariate Rician shadowed distributed random variables (RVs), $H_{v,1}$ and $H_{v,2}$, is modeled as [26]:

$$H_{v,k} = \sigma_v \sqrt{1-\rho_v} X_k + \sigma \sqrt{\rho_v} X_0 + Z_v, \tag{3}$$

where v is the downlink UAV index, $X_k, k \in \{0,1,2\}$ are Gaussian RVs with zero mean and variance $\frac{1}{2}$, $E\left\{(\sigma_v \sqrt{1-\rho_v} X_k + \sigma_v \sqrt{\rho_v} X_0)^2\right\} = \sigma_v^2$ represents the variance of the diffuse components [26], $0 \le \rho_v \le 1$ is the cross correlation coefficient between the diffuse components, and $E\{\bullet\}$ is the statistical expectation operator. Finally, the RV Z_v follows a Nakagami-m distribution with shaping parameter $m_v \ge 0.5$ and $E\{|Z_v|^2\} = \Omega_{N,v}$. The RV Z_v represents the severity of shadowing on the LOS component [26]. Hence, a small m_v indicates severe LOS shadowing, i.e., small Rician K factor, while a very large m_v corresponds to near-LOS conditions, i.e., no LOS shadowing and large Rician K factor. Therefore, conditions captured on LOS links via other channel models, e.g., Nakagami-m model, can also be captured using the bivariate Rician shadowed fading model.

A. Derivation of the Joint PDF and Joint CDF

Defining $R_{v,k} = |H_{v,k}|$, we note that the RV $R_{v,k}$ follows a bivariate Rician shadowed distribution with $E\{R_{v,k}^2\} = \sigma_v^2(1+K_v)$ and Rician factor $K_v = \frac{\Omega_{N,v}}{\sigma_v^2}$ for downlink UAV-v. From [26, eq. (4)], the joint PDF $f_{R_{v,1},R_{v,2}}(r_{v,1},r_{v,2})$ of $R_{v,k}$ is:

$$
\begin{aligned}
f_{R_{v,1},R_{v,2}}(r_{v,1},r_{v,2}) &= \frac{8\left(\frac{m_v \rho_v}{m_v \rho_v + K_v}\right)_v^m}{\sigma_v^6 \rho_v (1-\rho_v)^2} r_{v,1} r_{v,2} \\
&\times \exp\left(-\frac{r_{v,1}^2 + r_{v,2}^2}{\sigma_v^2(1-\rho_v)}\right) \int_0^\infty x \exp\left(\frac{-(1+\rho_v)}{\sigma_v^2 \rho_v (1-\rho_v)} x^2\right) \\
&\times I_0\left(\frac{2r_{v,1}}{\sigma_v^2(1-\rho_v)} x\right) I_0\left(\frac{2r_{v,2}}{\sigma_v^2(1-\rho_v)} x\right) \\
&\times {}_1F_1\left(m_v, 1; \frac{K_v}{\sigma_v^2 \rho_v (\rho_v m_v + K_v)} x^2\right) dx,
\end{aligned}
\tag{4}
$$

where $I_0(\bullet)$ is the modified Bessel function of the first kind with zero order [48, eq. (9.6.10)] and ${}_1F_1(\bullet)$ is the confluent Hypergeometric function [49].

The joint PDF expression in (4) may require the use of complicated numerical methods when evaluating commonly used performance metrics, e.g., outage probability or finite SNR diversity gain. We present an alternative closed-form expression for $f_{R_{v,1},R_{v,2}}(r_{v,1},r_{v,2})$ in the following Lemma:

Lemma 1: The closed-form expression for $f_{R_{v,1},R_{v,2}}(r_{v,1},r_{v,2})$ can be expressed as the following power series:

$$
\begin{aligned}
&f_{R_{v,1},R_{v,2}}(r_{v,1},r_{v,2}) \\
&\approx \sum_{k=0}^{K_{tr,1}} \sum_{i=0}^{k} \sum_{n=0}^{i} \alpha(k,i,n) r_{v,1}^{2n+1} r_{v,2}^{2(i-n)+1} \exp\left(-\frac{r_{v,1}^2 + r_{v,2}^2}{\sigma_v^2(1-\rho_v)}\right),
\end{aligned}
\tag{5}
$$

where $\alpha(k,i,n) = \frac{8(m_v)_{k-i}\left(\frac{K_v}{\sigma_v^2 \rho_v (\rho_v m_v + K_v)}\right)^{k-i}\left(\frac{m_v \rho_v}{m_v \rho_v + K_v}\right)^{m_v}}{\Gamma^2(n+1)\Gamma^2(i-n+1)[\sigma_v^2(1-\rho_v)]^{2i}(1)_{k-i}(k-i)!\sigma_v^6 \rho_v}$
$\times \frac{k!}{2\left(\frac{1+\rho_v}{\sigma_v^2 \rho_v (1-\rho_v)}\right)^{k+1}(1-\rho_v)^2}$, $K_{tr,j}$ for $j \in \{1,2\}$ is the truncation

order, and $(a)_k = \frac{\Gamma(a+k)}{\Gamma(a)}$ is the Pochhammer symbol [48, eq. (6.1.22)].

Proof: The proof is provided in Appendix A ∎

As the subsequent analysis in the rest of this paper are based on the power series expression in (5), it is crucial to show that (5) is convergent. In the next Corollary, we show that the alternative closed-form expression for $f_{R_{v,1},R_{v,2}}(r_{v,1},r_{v,2})$ in (5) is convergent.

Corollary 1: The expression for $f_{R_{v,1},R_{v,2}}(r_{v,1},r_{v,2})$ in (5) has a convergence radius of ∞.

Proof: The proof is given in Appendix B. ∎

As a result of Corollary 1, term-wise integration and differentiation can be performed on the power series expression in (5) [49], [50]. Therefore, the closed-form joint CDF $F_{R_{v,1},R_{v,2}}(\gamma_1, \gamma_2)$ can also be obtained from (5) as shown in the following Lemma:

Lemma 2: The closed-form expressions for $F_{R_{v,1},R_{v,2}}(\gamma_1, \gamma_2)$ can be expressed as:

$$
\begin{aligned}
&F_{R_{v,1},R_{v,2}}(\gamma_1, \gamma_2) \\
&\approx \sum_{k=0}^{K_{tr,1}} \sum_{i=0}^{k} \sum_{n=0}^{i} \sum_{l=0}^{K_{tr,2}} \sum_{q=0}^{l} \alpha(k,i,n)G(l,n,i,q) \\
&\qquad\qquad \times (\gamma_1)^{2(q+n+1)}(\gamma_2)^{2(l-q+i-n+1)},
\end{aligned}
\tag{6}
$$

where $G(l,n,i,q) = \frac{(-1)^l \binom{l}{q}}{[\sigma_v^2(1-\rho_v)]^l l! 4(q+n+1)(l-q+i-n+1)}$.

Proof: The proof is provided in Appendix C. ∎

Compared to the expression of $F_{R_{v,1},R_{v,2}}(\gamma_1, \gamma_2)$ given in [26, eq. (23)], (6) demonstrates that $F_{R_{v,1},R_{v,2}}(\gamma_1, \gamma_2)$ can be evaluated in closed-form. Furthermore, (6) is presented in a desirable form, as term-wise integration and differentiation can be conducted using the presented power series expression. As it will be shown, (6) enables the tractable derivation of the NOMA-aided UCS outage probability and diversity gain under the BPP model, which may not be possible using [26, eq. (23)].

B. Truncation Analysis of the Joint PDF and Joint CDF

It is worth noting that Corollary 1 is evaluated by applying the D'Alembert test on k, i, and n in (5). Since the D'Alembert test indicates a convergence radius of ∞, the same technique can also be extended to determine the truncation error $(\mathcal{T}_\epsilon)$ of the joint PDF $f_{R_{v,1},R_{v,2}}(r_{v,1},r_{v,2})$ in (5). In particular, $\mathcal{T}_\epsilon$ can be defined as [43, eq. (92)]:

$$
\begin{aligned}
\mathcal{T}_\epsilon &= \sum_{k=K_{tr,1}+1}^{\infty} \sum_{i=0}^{K_{tr,1}} \sum_{n=0}^{i} \alpha(k,i,n) \\
&\qquad \times r_{v,1}^{2n+1} r_{v,2}^{2(i-n)+1} \exp\left(-\frac{r_{v,1}^2 + r_2^2}{\sigma_v^2(1-\rho_v)}\right).
\end{aligned}
\tag{7}
$$

From (7), we present an upper bound of the truncation error $(\mathcal{T}_{\epsilon,upper})$ for the joint PDF $f_{R_{v,1},R_{v,2}}(r_{v,1},r_{v,2})$ in (5) in the next Lemma:

Lemma 3: For a sufficiently large truncation order $(K_{tr,1})$, the upper bound of the truncation error in (5) is:

$$\mathcal{T}_{\epsilon,upper} = \sum_{i=0}^{K_{tr,1}} \sum_{n=0}^{i} \frac{\alpha(K_{tr,1},i,n)}{1-\Delta(K_{tr,1})}$$
$$\times r_{v,1}^{2n+1} r_{v,2}^{2(i-n)+1} \exp\left(-\frac{r_{v,1}^2+r_{v,2}^2}{\sigma_v^2(1-\rho_v)}\right), \quad (8)$$

where $\Delta(k) = \left(\frac{K_v}{\sigma_v^2 \rho_v (\rho_v m_v + K_v)}\right)^{\frac{1}{k}}$.

Proof: The proof is provided in Appendix D ∎

The expression in (8) is useful in determining the necessary value of $K_{tr,1}$ that satisfies $\mathcal{T}_{\epsilon,upper} < \epsilon$, where ϵ is an error threshold value, for varying values of the Rician K factor, m_v, σ_v, and ρ_v. It is important to note that the accuracy of $\mathcal{T}_\epsilon$ and $\mathcal{T}_{\epsilon,upper}$ improves when a sufficiently large $K_{tr,1}$ is chosen [43]. Thus, when the value chosen for $K_{tr,1}$ is insufficient, $\mathcal{T}_\epsilon$ and $\mathcal{T}_{\epsilon,upper}$ may not be accurate and $K_{tr,1}$ should be incremented [43]. From (8), the behavior of $\mathcal{T}_{\epsilon,upper}$ with respect to the Rician K factor, m_v, σ_v, and ρ_v is given in the following Corollaries:

Corollary 2: Increasing m_v, σ_v, or ρ_v leads to a smaller $\mathcal{T}_{\epsilon,upper}$.

Proof: From (8), it is noted that m_v, σ_v, and ρ_v are in the denominator of $\Delta(k)$. Therefore, $\Delta(k) \to 0$ when m_v, σ_v, or ρ_v is increased. This completes the proof. ∎

Corollary 3: As the Rician K factor increases, a sufficiently large $K_{tr,1}$ is needed in order to reduce $\mathcal{T}_{\epsilon,upper}$.

Proof: From (8), it is seen that $\lim_{k\to\infty} \Delta(k) = \frac{1}{k} \lim_{k\to\infty} \frac{K_v}{\sigma_v^2 \rho_v (\rho_v m_v + K_v)} = \frac{1}{k}$. Therefore, as the Rician K factor increases, $\Delta(k) \to 0$ only when $K_{tr,1}$ is sufficiently large. This completes the proof. ∎

The impact of the Rician K factor, LOS shadowing severity (m_v), variance of the diffuse components (σ_v^2), and cross correlation (ρ_v) on $\mathcal{T}_{\epsilon,upper}$ is established in Corollaries 2 and 3. For instance, Corollary 2 shows that the upper bound of the joint PDF truncation error $\mathcal{T}_{\epsilon,upper}$ in (8) decreases when LOS shadowing is light, i.e., m_v is large, variance of the diffuse components (σ_v^2) is large, or when cross correlation (ρ_v) is high. Also, Corollary 3 shows that the joint PDF of bivariate Rician shadowed fading channels with large Rician K factor requires a sufficiently large truncation order $K_{tr,1}$ in order to attain a lower $\mathcal{T}_{\epsilon,upper}$. Furthermore, smaller $K_{tr,1}$ can be used when (5) is used to model a bivariate Rayleigh shadowed fading environment, i.e., Rician K factor is zero. [7] Furthermore, Corollaries 2 and 3 can also be used to provide an indication of the necessary $K_{tr,1}$ for varying values of the Rician K factor, m_v, σ_v, and ρ_v.

The approach in Lemma 3 and Corollaries 2 and 3 can also be used to analyze the truncation error (e) of the joint CDF $F_{R_{v,1},R_{v,2}}(\gamma_1,\gamma_2)$ in (6). Specifically, e can be defined as [43, eq. (82)]:

$$e = \sum_{k=0}^{K_{tr}} \sum_{i=0}^{k} \sum_{n=0}^{i} \sum_{l=K_{tr}+1}^{\infty} \sum_{q=0}^{l} \mu(k,l)$$

$$+ \sum_{k=K_{tr}+1}^{\infty} \sum_{i=0}^{k} \sum_{n=0}^{i} \sum_{l=0}^{K_{tr}} \sum_{q=0}^{l} \mu(k,l)$$
$$+ \sum_{k=K_{tr}+1}^{\infty} \sum_{i=0}^{k} \sum_{n=0}^{i} \sum_{l=k}^{\infty} \sum_{q=0}^{l} \mu(k,l)$$
$$+ \sum_{l=K_{tr}+1}^{\infty} \sum_{q=0}^{l} \sum_{k=l}^{\infty} \sum_{i=0}^{k} \sum_{n=0}^{i} \mu(k,l), \quad (9)$$

where $K_{tr,1} = K_{tr,2} = K_{tr}$ and $\mu(k,l) = \alpha(k,i,n)G(l,n,i,q)(\gamma_1)^{2(q+n+1)}(\gamma_2)^{2(l-q+i-n+1)}$. From (9), the upper bound of the truncation error (e_{upper}) for the joint CDF $F_{R_{v,1},R_{v,2}}(\gamma_1,\gamma_2)$ in (6) is presented in the next Lemma:

Lemma 4: For a sufficiently large truncation order (K_{tr}), the upper bound of the truncation error in (6) is:

$$e_{upper} = \sum_{k=0}^{K_{tr}} \sum_{i=0}^{k} \sum_{n=0}^{i} \sum_{q=0}^{K_{tr}+1} \frac{\mu(k,K_{tr}+1)}{1-\Theta_1(k,K_{tr}+1)}$$
$$+ \sum_{i=0}^{K_{tr}} \sum_{n=0}^{i} \sum_{l=0}^{K_{tr}} \sum_{q=0}^{l} \frac{\mu(K_{tr},l)}{1-\Theta_2(K_{tr})}$$
$$+ \sum_{k=K_{tr}+1}^{\infty} \sum_{i=0}^{k} \sum_{n=0}^{i} \sum_{q=0}^{K_{tr}+1} \frac{\mu(k,K_{tr}+1)}{1-\Theta_1(k,K_{tr}+1)}$$
$$+ \sum_{q=0}^{K_{tr}+1} \sum_{i=0}^{K_{tr}} \sum_{n=0}^{i} \frac{\mu(K_{tr},K_{tr}+1)}{1-\Theta_2(K_{tr})}, \quad (10)$$

where $\Theta_1(k,l) = \frac{(-1)(\gamma_2)^2(l+1)(l-q+i-n+1)}{\sigma_v^2(1-\rho_v)l^2(l-q+i-n+2)}$ and $\Theta_2(k) = \Delta(k) = \left(\frac{K_v}{\sigma_v^2 \rho_v (\rho_v m_v + K_v)}\right)^{\frac{1}{k}}$.

Proof: The proof is provided in Appendix E ∎

Similar to (8), the upper bound in (10) can be used to identify the necessary value of K_{tr} such that $e_{upper} < \epsilon$, where ϵ is an error threshold value, for varying values of the Rician K factor, m_v, σ_v, ρ_v, and γ_2. Also, the accuracy of e and e_{upper} improves when a sufficiently large $K_{tr,1}$ is chosen [43]. When an insufficient value is chosen for $K_{tr,1}$, e and e_{upper} may not be accurate and $K_{tr,1}$ should be incremented [43]. From (10), the behavior of e_{upper} with respect to ρ_v and γ_2 is given in the following Corollary:

Corollary 4: Increasing ρ_v or decreasing γ_2 leads to a smaller e_{upper}.

Proof: From (10), it is noted that ρ_v is in the denominator of $\Theta_1(k,l)$. Likewise, γ_2 is in the numerator of $\Theta_1(k,l)$. Therefore, $\Theta_1(k,l) \to 0$ when ρ_v is increased or when γ_2 is decreased. This completes the proof. ∎

The impact of ρ_v and γ_2 on e_{upper} is established in Corollary 4. Hence, one can now use Corollary 4 to decide on the choice of K_{tr} to obtain $e_{upper} < \epsilon$ based on ρ_v and γ_2. It should also be noted that Corollaries 2 and 3 are also applicable to (10).

IV. OUTAGE PROBABILITY DERIVATIONS

In this section, the NOMA outage probability expression for downlink UAV-j employing selection combining is presented. The OMA outage probability expression for downlink UAV-j

---

[7]To see this, Rician factor $K_v = \frac{\Omega_{N_v}}{\sigma_v^2} = 0$ implies that $\Omega_{N_v} = 0$, i.e., the RV Z_v in (3) is nonexistent.

is also provided as a benchmark. Let the transmission rate of the GS be defined as $\mathcal{R}^x$, where $x \in \{NOMA, OMA\}$. For a fair comparison between NOMA and OMA, we let $\mathcal{R}^{NOMA} = \frac{1}{N_D} \mathcal{R}^{OMA}$.

A. Downlink NOMA Outage Probability

At downlink UAV-j, let the selection combining NOMA outage event $\left(O_j^{NOMA}\right)$ be defined as:

$$O_j^{NOMA} = \left\{ R_{j,l}, d_j : \max\left(R_{j,1}, R_{j,2}\right) < \gamma_j^{NOMA} \sqrt{\frac{d_j^L}{P_r}} \right\}, \quad (11)$$

where $\gamma_j^{NOMA} = \sqrt{\frac{2^{\mathcal{R}^{NOMA}} - 1}{a_j - \left(\sum_{i=1}^{j-1} a_i\right)\left(2^{\mathcal{R}^{NOMA}} - 1\right)}}$ is the NOMA threshold such that $R^{NOMA} < \log_2\left(1 + \frac{a_j}{\sum_{i=1}^{j-1} a_i}\right)$. [8] Then, the closed-form downlink NOMA outage probability expression for UAV-j is presented in the following Theorem.

Theorem 1: The NOMA outage probability at downlink UAV-j is:

$$Pr\left(O_j^{NOMA}\right) \approx \sum_{k=0}^{K_{tr,1}} \sum_{i=0}^{k} \sum_{n=0}^{i} \sum_{l=0}^{K_{tr,2}} \sum_{q=0}^{l} \alpha(k, i, n) G(l, n, i, q)$$
$$\times \Xi_j(l, i) \left[\frac{\left(\gamma_j^{NOMA}\right)^2}{P_r}\right]^{2+l+i}, \quad (12)$$

where $\Xi_j(l, i) = \frac{2\left[\left(L_{p,j}\right)^{L(2+l+i)+2} - \left(L_{m,j}\right)^{L(2+l+i)+2}\right]}{r_a^2 \left[L(2+l+i)+2\right]}$.

Proof: The proof is provided in Appendix F. ∎

In Theorem 1, the effects of correlation, shadowing, and the Rician K factors on the SOIs at the UAVs are mostly captured in the functions $\alpha(k, i, n)$ and $G(l, n, i, q)$. Similarly, the effects of the GS transmission rate and NOMA power allocation factor on outage probability are reflected in γ_j^{NOMA}, while the function $\Xi_j(l, i)$ in Theorem 1 captures the stochastic geometry behavior of the UAV spatial locations. Specifically, $\Xi_j(l, i)$ reflects the effect of the BPP model in the close-form outage probability expression. Thus, using Theorem 1, the reliability of downlink NOMA can be analyzed within the BPP model for UCSs.

It is also worth emphasizing that the normalized average received power (P_r) appears in the denominator of (12). As it will be shown subsequently, (12) indicates the absence of an outage probability error floor in $Pr\left(O_j^{NOMA}\right)$ for downlink NOMA over correlated Rician shadowed fading channels.

B. Downlink OMA Outage Probability

As compared to NOMA, the GS transmits data to the downlink UAVs over separate time-frequency resources in OMA transmission schemes. Let the instantaneous SNR of the lth receive antenna at downlink UAV-j be $SNR_{j,l} = P_r d_j^{-L} |R_{j,l}|^2$.

---

[8]It is important to note that the NOMA threshold varies for each UAV due to the power allocation factors, SIC, and the considered BPP model.

Also, let the selection combining OMA outage event $\left(O_j^{OMA}\right)$ be defined as:

$$O_j^{OMA} = \left\{ R_{j,l}, d_j : \max\left(R_{j,1}, R_{j,2}\right) < \gamma_j^{OMA} \sqrt{\frac{d_j^L}{P_r}} \right\}, \quad (13)$$

where $\gamma_j^{OMA} = \sqrt{2^{\mathcal{R}^{OMA}} - 1}$ is the OMA threshold. Then, the closed-form OMA outage probability expression for UAV-j is given in the next Theorem.

Theorem 2: The OMA outage probability at downlink UAV-j is:

$$Pr\left(O_j^{OMA}\right) \approx \sum_{k=0}^{K_{tr,1}} \sum_{i=0}^{k} \sum_{n=0}^{i} \sum_{l=0}^{K_{tr,2}} \sum_{q=0}^{l} \alpha(k, i, n) G(l, n, i, q)$$
$$\times \Xi_j(l, i) \left[\frac{\left(\gamma_j^{OMA}\right)^2}{P_r}\right]^{2+l+i}. \quad (14)$$

Proof: The expression in (14) is obtained using the same approach in Appendix F. ∎

Although one can also invoke [26, eq. (48)] to evaluate $Pr\left(O_j^{OMA}\right)$, tractable analytical expressions may not be possible once the BPP model is considered. In contrast, we demonstrate in (14) that evaluating $Pr\left(O_j^{OMA}\right)$ within the BPP model can be achieved in a straightforward fashion using Lemma 2.

V. FINITE SNR DIVERSITY GAIN DERIVATIONS

The finite SNR diversity gain expressions for downlink NOMA and uplink NOMA are presented in this section. We also present finite SNR diversity gain expressions for OMA in this section.

The finite SNR diversity gain d_f of a given system quantifies the decay of outage probability at low to moderate SNR regimes [36], [37]. In particular, the finite SNR diversity gain is defined as [36, eq. (5)]:

$$d_f = \frac{-P_r}{Pr(O)} \frac{\partial}{\partial P_r} Pr(O), \quad (15)$$

where O and $Pr(O)$ are the considered outage event and outage probability, respectively. From [37] and [42], one obtains the asymptotic diversity gain, defined in [39], by evaluating (15) at high SNR regimes. In this spirit, finite SNR analysis is employed to investigate the impact of MUI in downlink NOMA for UAV communications.

A. Downlink NOMA Finite SNR Diversity Gain

Let the downlink NOMA finite SNR diversity gain at UAV-j be $d_{f,j}^{NOMA}$. Then, the closed-form expression for $d_{f,j}^{NOMA}$ is presented in the following Proposition.

Proposition 1: The downlink NOMA finite SNR diversity gain at UAV-j is:

$$d_{f,j}^{NOMA} \approx \frac{-P_r}{Pr(O_j^{NOMA})} \sum_{k=0}^{K_{tr,1}} \sum_{i=0}^{k} \sum_{n=0}^{i} \sum_{l=0}^{K_{tr,2}} \sum_{q=0}^{l} \alpha(k, i, n)$$
$$\times G(l, n, i, q) \Xi_j(l, i) \frac{\left(\gamma_j^{NOMA}\right)^{2(2+l+i)}(-2-l-i)}{(P_r)^{3+l+i}}. \quad (16)$$

Proof: Equation (16) can be obtained from (12) by applying (15). It should be noted that the differentiation conducted as a result of deriving (16) is valid due to Corollary 1 [49], [50]. ∎

As (12) is presented in a desirable form, i.e., as a power series, one can obtain a closed-form expression of $d_{f,j}^{NOMA}$ in (16), which may not be tractable using the expression in [26, eq. (48)]. Furthermore, the expression in (16) quantifies the NOMA outage probability decay of downlink UAV-j as a function of P_r while $\Xi_j(l, i)$ reflects the effect of the BPP model on finite SNR diversity gain. Thus, a larger $d_{f,j}^{NOMA}$ indicates a steeper drop in $Pr(O_j^{NOMA})$ as P_r varies.

Using Proposition 1, one also arrives at the asymptotic NOMA diversity gain for downlink UAV-j in the following Corollary.

Corollary 5: At asymptotic SNR regimes, NOMA achieves full diversity gain at downlink UAV-j, i.e., $d_{f,j}^{NOMA} = 2$.

Proof: The proof is provided in Appendix G. ∎

Corollary 5 shows that the NOMA-aided UCS is not interference-limited when employing downlink NOMA, despite the presence of MUI from the SOIs of other downlink UAVs. Furthermore, $d_{f,j}^{NOMA}$ is not affected by ρ_v at high P_t regimes.

B. Downlink OMA Finite SNR Diversity Gain

Let the downlink OMA finite SNR diversity gain at UAV-j be $d_{f,j}^{OMA}$. Then, the closed-form expression for $d_{f,j}^{OMA}$ is presented in the following Proposition.

Proposition 2: The downlink OMA finite SNR diversity gain at UAV-j is:

$$d_{f,j}^{OMA} \approx \frac{-P_r}{Pr(O_j^{OMA})} \sum_{k=0}^{K_{tr,1}} \sum_{i=0}^{k} \sum_{n=0}^{i} \sum_{l=0}^{K_{tr,2}} \sum_{q=0}^{l} \alpha(k, i, n)$$
$$\times G(l, n, i, q) \Xi_j(l, i) \frac{\left(\gamma_j^{OMA}\right)^{2(2+l+i)}(-2-l-i)}{(P_r)^{3+l+i}} \quad (17)$$

Proof: The closed-form expression in (17) is obtained using the same approach in Appendix G. ∎

Similar to Proposition 1, one obtains the asymptotic OMA diversity gain for downlink UAV-j using Proposition 2 as shown in the following Corollary.

Corollary 6: At asymptotic SNR regimes, OMA achieves full diversity gain at downlink UAV-j, i.e., $d_{f,j}^{OMA} = 2$.

Proof: Corollary 6 is proven in the same manner as Corollary 5. ∎

Using Proposition 2, the finite SNR diversity gain of OMA transmissions at downlink UAV-j with selection combining can now be analyzed over correlated Rician shadowed fading channels.

VI. NUMERICAL RESULTS

Numerical and simulation results pertaining to both NOMA-aided and OMA-based UCSs are presented in this section. Monte Carlo simulations were also conducted with 10^6 samples, based on simulation parameters provided in

TABLE I
SIMULATION PARAMETERS

| Parameter(s)	Value(s)
Number of Downlink UAVs	$N_D = 3$ [30], [51]
Rician K Factors	7 dB [1, Table V] for $\sigma = 1$
Shaping Parameter	$m = 5$ [52]
Transmit Power	$0 \leq P_t \leq 30$ (dBm) [51]
Path Loss Exponent	$L = 2$ [1, Table III], [53]
Cross Correlation Coefficient	$\rho = 0.5$
Carrier Frequency	$f_c = 2$ GHz [51]
Bandwidth	$B_W = 10$ MHz [51]
Transmission rate	$\mathcal{R}^{OMA} = 0.1$ b/s/Hz
Radius	$r_a = 10$ km [47]
Minimum UAV Altitude	$h_{min} = 0.1$ km [51]
Altitude Separation Factor	$\overline{\omega} = 0.1$
Truncation Order	$K_{tr,1} = 30$, $K_{tr,2} = 40$
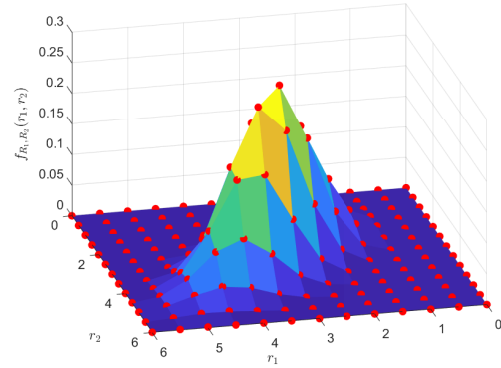
Fig. 2. Joint PDF comparison between the exact expression in [26, eq. (4)] (denoted in red markers) and the closed-form expression in (5) for $m = 10$, $K_{tr,1} = 150$, and Rician K factor of 10 dB.

Table I (unless otherwise stated) for $\sigma_v = \sigma$, $\rho_v = \rho$. [9] [10] It is also useful to recall that the downlink UAVs operate at different altitudes, i.e., $h_j < h_{j+1}$. Effectively, the Euclidean distance (d_j) between downlink UAV-j and the GS then becomes ranked such that $d_j < d_{j+1}$. For such distance-based ordering, the ranking of users based on distance enables an approximation of the respective ranked received signal powers at the receiver [55]–[57]. Also, in NOMA systems practicing distance-based user ordering, higher transmit powers are allocated to users that are further away to facilitate signal detection via SIC [58].

It should be emphasized that the present work employs the BPP model in [29], where D_j is a uniformly distributed RV, i.e., the horizontal Euclidean distance of all UAVs are independently and identically distributed. Although all downlink UAVs will on average have the same horizontal distance, $h_j < h_{j+1}$ implies that $d_j < d_{j+1}$. Accordingly, downlink UAVs at lower altitudes will on average be closer to the GS than downlink UAVs at higher altitudes.

---

[9] A LOS shadowing severity of $m = 5$, i.e., shaping parameter, was chosen to reflect medium shadowing severity in a suburban environment [52].

[10] Channel measurement campaigns have shown that $1.5 \leq L \leq 2$ in the suburban environment, while UAV altitudes between 0.3 km and 1 km was noted in [54].
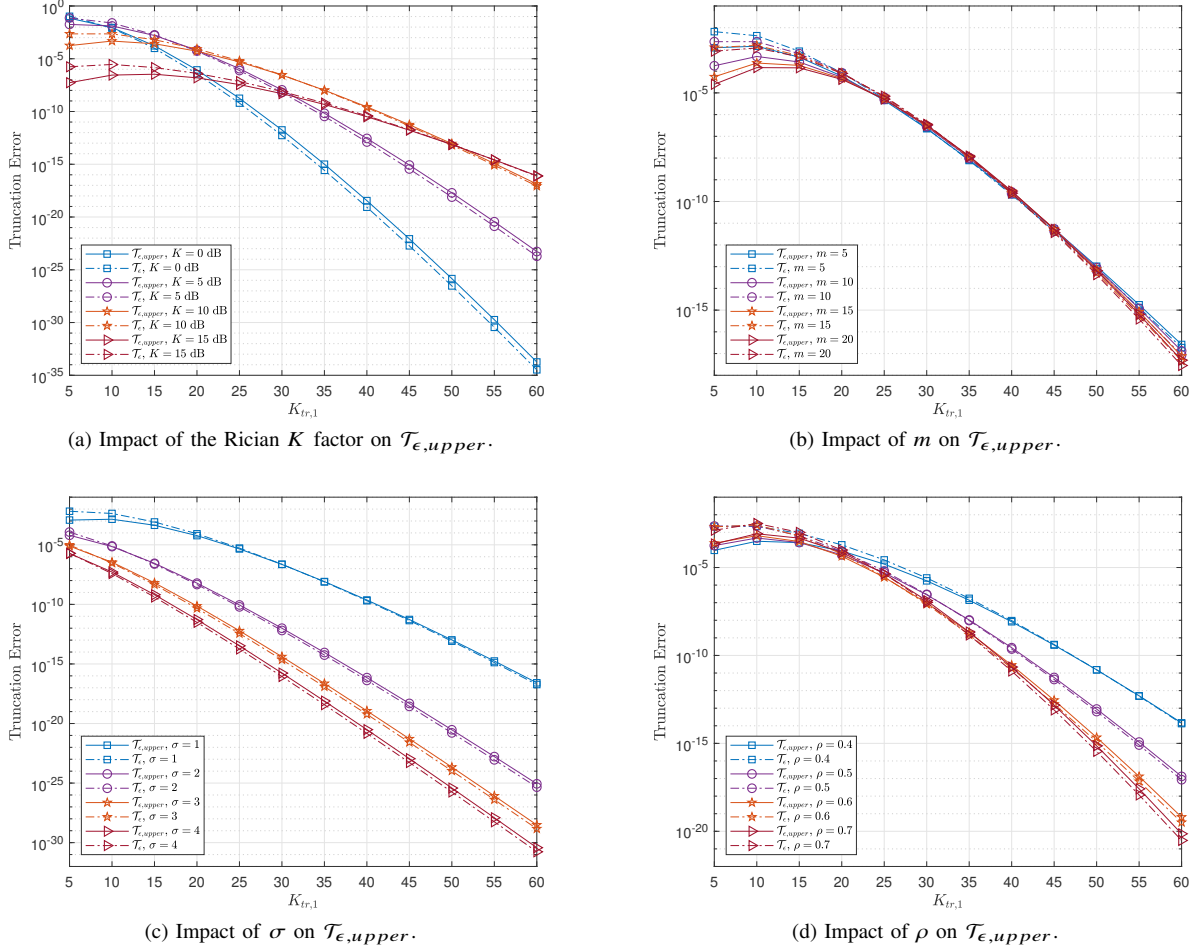
(a) Impact of the Rician K factor on $\mathcal{T}_{\epsilon,upper}$.

(b) Impact of m on $\mathcal{T}_{\epsilon,upper}$.

(c) Impact of σ on $\mathcal{T}_{\epsilon,upper}$.

(d) Impact of ρ on $\mathcal{T}_{\epsilon,upper}$.

Fig. 3. Impact of the Rician K factor, m, σ, and ρ on $\mathcal{T}_{\epsilon,upper}$ for $r_{v,1} = r_{v,2} = 1$ and Rician K factor of 10 dB.
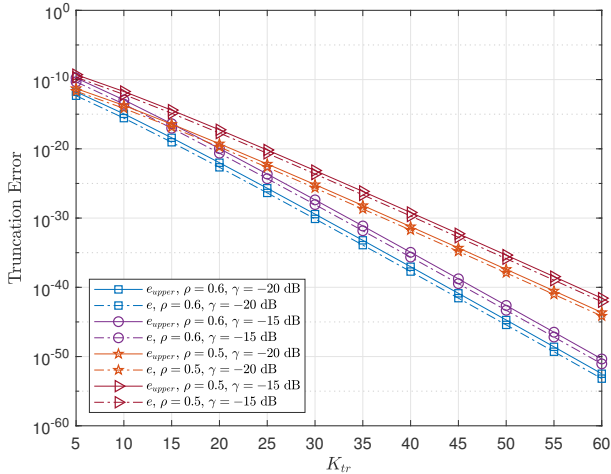

Fig. 4. Impact of ρ and γ on e_{upper} for $\gamma_1 = \gamma_2 = -10$ dB and Rician K factor of 7 dB.

away from the GS [58], i.e., $a_j < a_{j+1}$. [11] Doing so allows downlink UAV-j to recover the SOI by performing SIC to remove MUI from downlink UAV-m for $m > j$, while ignoring MUI from DL UAV-k for $k < j$ [59], [60].

For the rest of the section, we present observations and discussions pertaining to the performance analysis of the NOMA-aided UCS.

A. Joint PDF Validation and Truncation Analysis

Fig. 2 shows a comparison between the closed-form joint PDF expression in (5) and the exact expression in [26, eq. (4)]. Evidently, (5) is validated as it is shown to be in very close agreement with [26, eq. (4)]. Furthermore, as $m \to \infty$, the closed-form expression in (5) can be used to model a bivariate Rician fading PDF.

The impact of the Rician K factor, m, σ, and ρ on the upper bound of the truncation error $\left(\mathcal{T}_{\epsilon,upper}\right)$ is shown

[11]While power allocation can be based on the horizontal Euclidean distance and altitude of the UAVs, such an approach may lead to high overheads for the NOMA-aided UCS. Furthermore, performance analysis of the NOMA-aided UCS becomes intractable. Instead, it is more practical to base a_j on h_j, i.e., only altitude, as transmissions to UAVs at higher altitude can be allocated a higher transmit power to overcome the effects of fading, shadowing, and cross correlation.

As such, the power allocation factor a_j is heuristically defined based on the altitudes of the N_D downlink UAVs to ensure fairness. Specifically, we let $a_j = \frac{h_j}{\sum_{k=1}^{N_D} h_k}$ in order to assign higher transmit powers to UAVs operating far
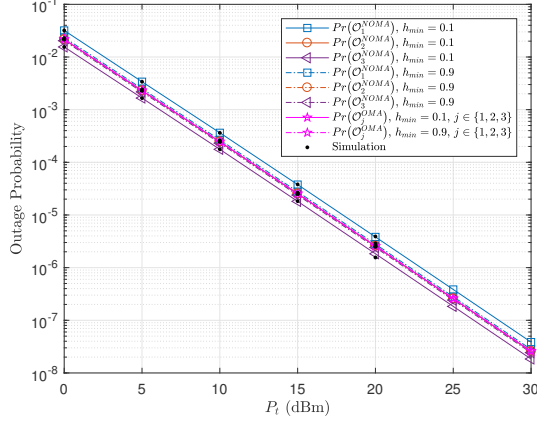
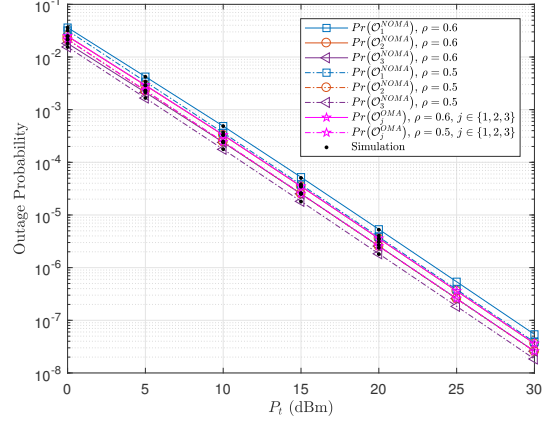Fig. 5. Impact of minimum altitude h_{min} on NOMA outage probability.

Fig. 6. Impact of cross correlation coefficient ρ on NOMA outage probability.

in Fig. 3. Likewise, the impact of ρ and γ on the upper bound of the truncation error (e_{upper}) is plotted in Fig. 4. In particular, it is seen in Fig. 3 and Fig. 4 that Lemmas 3 and 4 are validated, since $\mathcal{T}_\epsilon < \mathcal{T}_{\epsilon,upper}$ and $e < e_{upper}$ when $K_{tr,1}$ and K_{tr} are sufficiently large. Also, Fig. 3 shows that a small $K_{tr,1}$ leads to an insufficient number of terms to achieve convergence in the power series expressions, e.g., (5), (7), and (8). Such an observation is due to an insufficient value chosen for $K_{tr,1}$ to achieve the necessary accuracy, e.g., $\mathcal{T}_{\epsilon,upper} < \epsilon$. Nonetheless, the accuracy of $\mathcal{T}_\epsilon$ and $\mathcal{T}_{\epsilon,upper}$ improves as $K_{tr,1}$ is incremented. Thus, it can also be observed in Fig. 3 that $\mathcal{T}_\epsilon > \mathcal{T}_{\epsilon,upper}$ at the lower range of $K_{tr,1}$ and $\mathcal{T}_\epsilon \leq \mathcal{T}_{\epsilon,upper}$ at the higher range of $K_{tr,1}$. From Fig. 3a, it is seen that a larger $K_{tr,1}$ is needed to reduce $\mathcal{T}_{\epsilon,upper}$ as the Rician K factor increases. It is also observed in Fig. 3b, Fig. 3c, and Fig. 3d that an increase in m, σ, and ρ leads to a decrease in $\mathcal{T}_{\epsilon,upper}$. Similarly, Fig. 4 shows that an increase in ρ or decrease in γ leads to a decrease in e_{upper} Therefore, Corollaries 2, 3, and 4 are validated.

B. Outage Probability and Finite SNR Diversity Gain Analysis

Observation 1: The NOMA-aided UCS can simultaneously support more downlink UAVs on the same spectrum than an OMA-based UCS while achieving almost similar reliability.

Observation 2: Smaller cross correlation corresponds to higher reliability for both NOMA and OMA transmissions.

The impact of the minimum altitude (h_{min}) on the NOMA outage probability of downlink UAV-j $\left(Pr\left(O_j^{NOMA}\right)\right)$ is plotted in Fig. 5 for $1 \leq j \leq N_D$.

It is observed that $Pr\left(O_j^{NOMA}\right)$ is not limited by MUI, despite interference from the SOIs of other downlink UAVs. It is also seen that $Pr\left(O_3^{NOMA}\right) < Pr\left(O_2^{NOMA}\right) < Pr\left(O_1^{NOMA}\right)$ when $h_{min} = 0.1$ km, and $Pr\left(O_3^{NOMA}\right) \approx Pr\left(O_2^{NOMA}\right) \approx Pr\left(O_1^{NOMA}\right)$ when $h_{min} = 0.9$ km. Such an occurrence is due to the power allocation factor (a_j). Specifically, a low h_{min}, e.g., $h_{min} = 0.1$ km, results in a lower power allocation for UAV-1 (a_1) and a higher power allocation for UAV-3 (a_3). In contrast, a high h_{min}, e.g., $h_{min} = 0.9$ km, results in a more even power allocation for the UAVs, i.e., $a_1 \approx a_2 \approx a_3$. As h_{min} increases, the difference between a_j and a_{j+1} diminishes
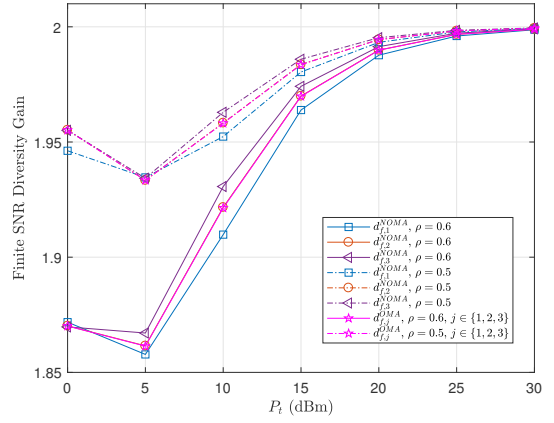

Fig. 7. Impact of cross correlation coefficient ρ on NOMA finite SNR diversity gain.

due to the altitude separation factor $(\overline{\omega})$. Thus, the downlink UAVs exhibit very similar NOMA outage probabilities for $h_{min} = 0.9$. When compared against the OMA-based UCS, it is evident that the NOMA-aided UCS achieves similar outage probability particularly at high h_{min}. Therefore, the NOMA-aided UCS is able to achieve similar reliability to an OMA-based UCS while simultaneously supporting a greater number of downlink UAVs as all NOMA transmissions occur over the same time-frequency resource.

The impact of the cross correlation coefficient (ρ) on the NOMA outage probability of downlink UAV-j, i.e., $Pr\left(O_j^{NOMA}\right)$, is plotted in Fig. 6 for $1 \leq j \leq N_D$. It is seen that an increase in ρ corresponds to an increase in $Pr\left(O_j^{NOMA}\right)$ and $Pr\left(O_j^{OMA}\right)$. Such a behavior is due to the decrease in diversity gain, i.e., $d_{f,j}^{NOMA}$ and $d_{f,j}^{OMA}$, as cross correlation (ρ) increases [26].

A clearer picture of the outage probability decay behavior is seen in Fig. 7, where $d_{f,j}^{NOMA}$ and $d_{f,j}^{OMA}$ is plotted for $1 \leq j \leq N_D$. Specifically, similar trends are also observed in Fig. 7 at low P_t regimes, with both NOMA and OMA transmissions experiencing lower $d_{f,j}^{NOMA}$ and $d_{f,j}^{OMA}$, respectively, as ρ is increased. It should also be pointed out that it

is possible for $d_{f,j}^{NOMA}$ to be large, e.g., much greater than 2, due to the steep drop in NOMA outage probability as P_t is increased. However, at high P_t regimes, it is observed that the impact of ρ diminishes since both $d_{f,j}^{NOMA} \to 2$ and $d_{f,j}^{OMA} \to 2$ as P_t increases. Such an observation is due to the fact that ρ only affects the coding gain of selection combining techniques [61]. In particular, the coding gain of both NOMA and OMA transmissions increases as P_t increases at low P_t regimes. As a result, a lower $d_{f,j}^{NOMA}$ and $d_{f,j}^{OMA}$ is experienced when ρ is increased. However, at high P_t regimes, the increase in the coding gain becomes negligible. Hence, $d_{f,j}^{NOMA} = d_{f,j}^{OMA} = 2$ for $\rho \in \{0.5, 0.6\}$, which validate Corollaries 5 and 6. Therefore, it is demonstrated that a low cross correlation is required in order to achieve a lower outage probability for the NOMA-aided UCS. Additionally, the coding gain of selection combining for both NOMA and OMA transmissions becomes stagnant at high P_t regimes.

VII. CONCLUSION

A NOMA-aided UCS with selection combining dual-diversity receivers is investigated in this paper as a step towards addressing spectrum scarcity in UAV communications. Through new closed-form expressions for the joint PDF and joint CDF, new expressions for the outage probability and finite SNR diversity gain of the NOMA-aided UCS are presented. It is shown that more downlink UAVs can be supported on the same spectrum with the NOMA-aided UCS, with an outage probability that is similar to OMA-based UCSs. Furthermore, the effect of cross correlation is analyzed, where it is shown that a lower cross correlation leads to lower outage probability in the NOMA-aided UCS. Also, it is demonstrated that correlation only reduces the diversity gain of NOMA-aided and OMA-based UCSs at low SNR regimes. Therefore, NOMA-aided UCSs are an attractive alternative over OMA-based schemes in future wireless systems.

APPENDIX A
PROOF OF LEMMA 1

We first begin by noting that $I_0\left(\frac{2r_{v,i}x}{\sigma_v^2(1-\rho_v)}\right)$ for $i = 1, 2$ in (4) can be represented as the following power series [48, eq. (9.6.10)]:

$$I_0\left(\frac{2r_{v,i}x}{\sigma_v^2(1-\rho_v)}\right) = \sum_{n=0}^{\infty} \frac{(1/4)^n}{n!\Gamma(n+1)}\left(\frac{2r_{v,i}x}{\sigma_v^2(1-\rho_v)}\right)^{2n}$$
$$= \sum_{n=0}^{\infty} C_i(n). \quad (18)$$

Then, using the Cauchy product theorem [49, eq. (0.316)], $\prod_{i=1}^{2} I_0\left(\frac{2r_{v,i}x}{\sigma_v^2(1-\rho_v)}\right)$ in (4) becomes:

$$\prod_{i=1}^{2} I_0\left(\frac{2r_{v,i}x}{\sigma_v^2(1-\rho_v)}\right) \approx \sum_{k=0}^{\infty}\sum_{n=0}^{k} C_1(n)C_2(k-n) \approx \sum_{k=0}^{K_{tr,1}} A(k), \quad (19)$$

where $A(k) = \sum_{n=0}^{k} \frac{(1/4)^k(2r_{v,1})^{2n}(2r_{v,2})^{2(k-n)}}{\Gamma^2(n+1)\Gamma^2(k-n+1)[\sigma_v^2(1-\rho_v)]^{2k}}x^{2k}$.

Next, $_1F_1\left(m_v, 1; \frac{K_v}{\sigma_v^2\rho_v(\rho_v m_v + K_v)}x^2\right)$ in (4) is also expressed as the following power series [48, eq. (13.1.2)]:

$$_1F_1\left(m_v, 1; \frac{K_v}{\sigma_v^2\rho_v(\rho_v m_v + K_v)}x^2\right) \approx \sum_{i=0}^{\infty} B(i), \quad (20)$$

where $B(i) = \frac{(m_v)_i}{i!(1)_i}\left(\frac{K_v}{\sigma_v^2\rho_v(m_v\rho_v + K_v)}\right)^i x^{2i}$. Using (19) and (20), along with the Cauchy product theorem [49, eq. (0.316)], $\prod_{i=1}^{2} I_0\left(\frac{2r_{v,i}x}{\sigma_v^2(1-\rho_v)}\right){}_1F_1\left(m_v, 1; \frac{K_v}{\sigma_v^2\rho_v(\rho_v m_v + K_v)}x^2\right)$ in (4) can be expressed as:

$$\prod_{i=1}^{2} I_0\left(\frac{2r_{v,i}x}{\sigma_v^2(1-\rho_v)}\right){}_1F_1\left(m_v, 1; \frac{K_v}{\sigma_v^2\rho_v(\rho_v m_v + K_v)}x^2\right)$$

$$\approx \sum_{k=0}^{K_{tr,1}}\sum_{i=0}^{k} A(i)B(k-i)$$

$$\approx \sum_{k=0}^{K_{tr,1}}\sum_{i=0}^{k}\sum_{n=0}^{i} \frac{(\frac{1}{4})^i(2r_{v,1})^{2n}(2r_{v,2})^{2(i-n)}}{\Gamma^2(n+1)\Gamma^2(i-n+1)[\sigma_v^2(1-\rho_v)]^{2i}(1)_{k-i}}$$

$$\times \frac{(m_v)_{k-i}}{(k-i)!}\left(\frac{K_v}{\sigma_v^2\rho_v(\rho_v m_v + K_v)}\right)^{k-i} x^{2k}. \quad (21)$$

Substituting (21) into (4) and utilizing the fact that $\int_0^{\infty} x^{2k+1}\exp\left(\frac{-(1-\rho_v)}{\sigma_v^2\rho_v(1-\rho_v)}x^2\right)dx = \frac{k!}{2}\left(\frac{1-\rho_v}{\sigma_v^2\rho_v(1-\rho_v)}\right)^{-(k+1)}$ [49, eq. (3.461.3)], one obtains the expression in (5). This completes the proof.

APPENDIX B
PROOF OF COROLLARY 1

To show that (5) is convergent, the D'Alembert test is invoked to show that $\lim_{n\to\infty} \frac{|\alpha(k,i,n+1)r_{v,1}^{2(n+1)+1}r_{v,2}^{2(i-n-1)+1}|}{|\alpha(k,i,n)r_{v,1}^{2n+1}r_{v,2}^{2(i-n)+1}|} = 0$, $\lim_{i\to\infty} \frac{|\alpha(k,i+1,n)r_{v,2}^{2(i-n+1)+1}|}{|\alpha(k,i,n)r_{v,2}^{2(i-n)+1}|} = 0$, and $\lim_{k\to\infty} \frac{|\alpha(k+1,i,n)|}{|\alpha(k,i,n)|} = 0$.

Starting with $\lim_{n\to\infty} \frac{|\alpha(k,i,n+1)r_{v,1}^{2(n+1)+1}r_{v,2}^{2(i-n-1)+1}|}{|\alpha(k,i,n)r_{v,1}^{2n+1}r_{v,2}^{2(i-n)+1}|}$, the limit can be evaluated as:

$$\lim_{n\to\infty} \frac{|\alpha(k,i,n+1)r_{v,1}^{2(n+1)+1}r_{v,2}^{2(i-n-1)+1}|}{|\alpha(k,i,n)r_{v,1}^{2n+1}r_{v,2}^{2(i-n)+1}|}$$

$$\overset{(a)}{=} \lim_{n\to\infty} \frac{r_{v,1}}{r_{v,2}^2}\left(\frac{n\Gamma(n)i^{1-n}\Gamma(i)}{n^2\Gamma(n)i^{-n}\Gamma(i)}\right)^2 = \lim_{n\to\infty} \frac{r_{v,1}}{r_{v,2}^2}\left(\frac{i}{n}\right)^2 = 0, (22)$$

where (a) is obtained using the asymptotic identity $\Gamma[m+n] \approx m^n\Gamma[m]$ in [62, eq. (25)].

For $\lim_{i\to\infty} \frac{|\alpha(k,i+1,n)r_{v,2}^{2(i-n+1)+1}|}{|\alpha(k,i,n)r_{v,2}^{2(i-n)+1}|}$, the limit is evaluated as:

$$\lim_{i\to\infty} \frac{|\alpha(k,i+1,n)r_{v,2}^{2(i-n+1)+1}|}{|\alpha(k,i,n)r_{v,2}^{2(i-n)+1}|}$$

$$\overset{(a)}{=} \lim_{i\to\infty} r_{v,2}^2\left(\frac{\Gamma(k-i-1+m_v)\left(\frac{K_v}{\sigma_v^2\rho_v(\rho_v m_v+K_v)}\right)^{k-i-1}}{\Gamma^2(i-n+2)[\sigma_v^2(1-\rho_v)]^{2i+2}\Gamma^2(k-i)}\right)$$

$$\times \left(\frac{\Gamma^2(i-n+1)[\sigma_v^2(1-\rho_v)]^{2i}\Gamma^2(k-i+1)}{\Gamma(k-i+m_v)\left(\frac{K_v}{\sigma_v^2\rho_v(\rho_v m_v+K_v)}\right)^{k-i}}\right)$$

$$\overset{(b)}{=} \lim_{i \to \infty} r_{v,2}^2 \left(\frac{k^{m_v - i - 1} \Gamma(k) \left(\frac{K_v}{\sigma_v^2 \rho_v (\rho_v m_v + K_v)} \right)^{k-i-1}}{i^{2-n} \Gamma(i) [\sigma_v^2 (1 - \rho_v)]^{2i+2} k^{-2i} \Gamma^2(k)} \right)$$

$$\times \left(\frac{i^{1-n} \Gamma(i) [\sigma_v^2 (1 - \rho_v)]^{2i} k^{-2i+2} \Gamma^2(k)}{k^{m_v - i} \Gamma(k) \left(\frac{K_v}{\sigma_v^2 \rho_v (\rho_v m_v + K_v)} \right)^{k-i}} \right)$$

$$= \lim_{i \to \infty} \frac{r_{v,2}^2 k}{\left(\frac{K}{\sigma_v^2 \rho_v (\rho_v m_v + K_v)} \right) i} = 0, \quad (23)$$

where (a) is due to $(a)_k = \frac{\Gamma(a+k)}{\Gamma(a)}$ [48, eq. (6.1.22)] and $(k - i)! = \Gamma(k - i + 1)$, and (b) is obtained using the asymptotic identity $\Gamma[m + n] \approx m^n \Gamma[m]$ in [62, eq. (25)].

Finally, for $\lim_{k \to \infty} \frac{|\alpha(k+1,i,n)|}{|\alpha(k,i,n)|}$, the limit is evaluated as:

$$\lim_{k \to \infty} \frac{|\alpha(k + 1, i, n)|}{|\alpha(k, i, n)|}$$

$$\overset{(a)}{=} \lim_{k \to \infty} \left(\frac{\Gamma(k - i + 1 + m_v) \left(\frac{K_v}{\sigma_v^2 \rho_v (\rho_v m_v + K_v)} \right)^{k+1-i}}{\Gamma^2(k - i + 2)} \right)$$

$$\times \left(\frac{\Gamma^2(k - i + 1)}{\Gamma(k - i + m_v) \left(\frac{K_v}{\sigma_v^2 \rho_v (\rho_v m_v + K)} \right)^{k-i}} \right)$$

$$\overset{(b)}{=} \lim_{k \to \infty} \left(\frac{K}{\sigma_v^2 \rho_v (\rho_v m_v + K_v)} \right)$$

$$\times \left(\frac{k^{m_v + 1 - i} \Gamma(k)}{[k^{2-i} \Gamma(k)]^2} \right) \left(\frac{[k^{1-i} \Gamma(k)]^2}{k^{m_v - i} \Gamma(k)} \right)$$

$$= \lim_{k \to \infty} \left(\frac{K_v}{\sigma_v^2 \rho_v (\rho_v m_v + K_v)} \right) \frac{1}{k} = 0, \quad (24)$$

where (a) is due to $(a)_k = \frac{\Gamma(a+k)}{\Gamma(a)}$ [48, eq. (6.1.22)] and $(k - i)! = \Gamma(k - i + 1)$, and (b) is obtained using the asymptotic identity $\Gamma[m + n] \approx m^n \Gamma[m]$ in [62, eq. (25)].

Thus, from (22), (23), and (24), the expression in (5) has a convergence radius of ∞. Therefore, (5) is shown to be convergent. This completes the proof.

APPENDIX C
PROOF OF LEMMA 2

We begin by noting that $\exp(x) \approx \sum_{l=0}^{K_{tr,2}} \frac{x^l}{l!}$ [49, eq. (1.211.1)]. Then, the joint CDF $F_{R_{v,1}, R_{v,2}}(\gamma_1, \gamma_2)$ can be obtained from (5) as follows:

$$F_{R_{v,1}, R_{v,2}}(\gamma_1, \gamma_2)$$

$$\overset{(a)}{\approx} \int_0^{\gamma_2} \int_0^{\gamma_1} \sum_{k=0}^{K_{tr,1}} \sum_{i=0}^{k} \sum_{n=0}^{i} \sum_{l=0}^{K_{tr,2}} \sum_{q=0}^{l} \alpha(k, i, n)$$

$$\times \frac{(-1)^l \binom{l}{q}}{l! [\sigma_v^2 (1 - \rho_v)]^l} (r_{v,1})^{2(q+n)+1} (r_{v,2})^{2(l-q+i-n)+1} dr_{v,1} dr_{v,2}$$

$$\overset{(b)}{\approx} \sum_{k=0}^{K_{tr,1}} \sum_{i=0}^{k} \sum_{n=0}^{i} \sum_{l=0}^{K_{tr,2}} \sum_{q=0}^{l} \alpha(k, i, n)$$

$$\times \frac{(-1)^l \binom{l}{q}}{l! [\sigma_v^2 (1 - \rho_v)]^l 4 (q + n + 1)(l - q + i - n + 1)}$$

$$\times (\gamma_1)^{2(q+n+1)} (\gamma_2)^{2(l-q+i-n+1)} \quad (25)$$

where (a) is obtained by applying the identities in [49, eq. (1.211.1)] and [49, eq. (1.111)], and (b) is obtained through term-wise intergration [49], [50]. This completes the proof.

APPENDIX D
PROOF OF LEMMA 3

The upper bound of the truncation error is obtained using the same approach in [43]. From the expression in (7), taking the ratio between terms $(\Delta(k))$ as k increases yields:

$$\Delta(k) = \frac{|\alpha(k + 1, i, n)|}{|\alpha(k, i, n)|} \overset{(a)}{=} \left(\frac{K_v}{\sigma_v^2 \rho_v (\rho_v m_v + K_v)} \right) \frac{1}{k} = 0, \quad (26)$$

where (a) is obtained from (24). Since $\Delta(k)$ monotonically decreases as $k \to \infty$, (7) becomes upper bounded by $\Delta(K_{tr,1})$ as shown [43, eq. (92)]:

$$\mathcal{T}_\epsilon \leq \sum_{i=0}^{K_{tr,1}} \sum_{n=0}^{i} \frac{\alpha(K_{tr,1}, i, n)}{1 - \Delta(K_{tr,1})}$$

$$\times r_{v,1}^{2n+1} r_{v,2}^{2(i-n)+1} \exp \left(- \frac{r_{v,1}^2 + r_{v,2}^2}{\sigma_v^2 (1 - \rho_v)} \right) \quad (27)$$

$$\leq \mathcal{T}_{\epsilon, upper}.$$

This completes the proof.

APPENDIX E
PROOF OF LEMMA 4

The upper bound of the truncation error e is obtained using the same approach in [43]. From (9), e can be rewritten as:

$$e = e_1 + e_2 + e_3 + e_4, \quad (28)$$

$$\text{where } e_1 = \sum_{k=0}^{K_{tr}} \sum_{i=0}^{k} \sum_{n=0}^{i} \sum_{l=K_{tr}+1}^{\infty} \sum_{q=0}^{l} \mu(k, l),$$

$$e_2 = \sum_{k=K_{tr}+1}^{\infty} \sum_{i=0}^{k} \sum_{n=0}^{i} \sum_{l=0}^{K_{tr}} \sum_{q=0}^{l} \mu(k, l),$$

$$e_3 = \sum_{k=K_{tr}+1}^{\infty} \sum_{i=0}^{k} \sum_{n=0}^{i} \sum_{l=k}^{\infty} \sum_{q=0}^{l} \mu(k, l),$$

$$e_4 = \sum_{l=K_{tr}+1}^{\infty} \sum_{q=0}^{l} \sum_{k=l}^{\infty} \sum_{i=0}^{k} \sum_{n=0}^{i} \mu(k, l).$$

Starting with e_1, taking the ratio between terms $(\Theta_1(k, l))$ as l increases yields:

$$\Theta_1(k, l) = \frac{\mu(k, l + 1)}{\mu(k, l)}$$

$$\overset{(a)}{=} \frac{(-1)(\gamma_2)^2 (l + 1)(l - q + i - n + 1)}{\sigma_v^2 (1 - \rho_v) l^2 (l - q + i - n + 2)} = 0, \quad (29)$$

where (a) is obtained through algebraic simplifications after applying the identities $\Gamma[m + n] \approx m^n \Gamma[m]$ [62, eq. (25)] and $\binom{x}{y} = \frac{\Gamma(x+1)}{\Gamma(y+1)\Gamma(x-y+1)}$ [48, eq. (3.1.2)]. Thereafter, e_1 is upper bounded as [43, eq. (89)]:

$$e_1 \leq \sum_{k=0}^{K_{tr}} \sum_{i=0}^{k} \sum_{n=0}^{i} \sum_{q=0}^{K_{tr}+1} \frac{\mu(k, K_{tr} + 1)}{1 - \Theta_1(k, K_{tr} + 1)}. \quad (30)$$

For e_2, taking the ratio between terms $(\Theta_2(k))$ as k increases yields:

$$\Theta_2(k) = \frac{\mu(k+1,l)}{\mu(k,l)} = \Delta(k) = 0,$$

where $\Delta(k)$ is given in (26). Then, e_2 can be upper bounded as [43, eq. (92)]:

$$e_2 \leq \sum_{i=0}^{K_{tr}} \sum_{n=0}^{i} \sum_{l=0}^{K_{tr}} \sum_{q=0}^{l} \frac{\mu(K_{tr},l)}{1-\Theta_2(K_{tr})}. \tag{31}$$

For e_3 and e_4, the upper bound can be respectively obtained from [43, eq. (93)] and [43, eq. (102)] as:

$$e_3 \leq \sum_{k=K_{tr}+1}^{\infty} \sum_{i=0}^{k} \sum_{n=0}^{i} \sum_{q=0}^{K_{tr}+1} \frac{\mu(k,K_{tr}+1)}{1-\Theta_1(k,K_{tr}+1)}, \tag{32}$$

$$e_4 \leq \sum_{q=0}^{K_{tr}+1} \sum_{i=0}^{K_{tr}} \sum_{n=0}^{i} \frac{\mu(K_{tr},K_{tr}+1)}{1-\Theta_2(K_{tr})}. \tag{33}$$

Then, combining (30), (31), (32), and (33) into (28) yields the upper bound in (10). This completes the proof.

APPENDIX F
PROOF OF THEOREM 1

From the selection combining NOMA outage event at downlink UAV-j (O_j^{NOMA}), the NOMA outage probability $(Pr(O_j^{NOMA}))$ can be obtained from the closed-form expression of $F_{R_{v,1},R_{v,2}}(\gamma_1,\gamma_2)$ in Lemma 2 as follows:

$$Pr(O_j^{NOMA})$$

$$= Pr\left(\max\left(R_{j,1}, R_{j,2}\right) < \gamma_j^{NOMA}\sqrt{\frac{d_j^L}{P_r}}\right)$$

$$= \int_{L_{m,j}}^{L_{p,j}} F_{R_{j,1},R_{j,2}}\left(\gamma_j^{NOMA}\sqrt{\frac{w^L}{P_r}}, \gamma_j^{NOMA}\sqrt{\frac{w^L}{P_r}}\right) f_{d_j}(w)\,dw$$

$$\approx \int_{L_{m,j}}^{L_{p,j}} \sum_{k=0}^{K_{tr,1}} \sum_{i=0}^{k} \sum_{n=0}^{i} \sum_{l=0}^{K_{tr,2}} \sum_{q=0}^{l} \alpha(k,i,n)G(l,n,i,q)$$

$$\times \left[\frac{(\gamma_j^{NOMA})^2}{P_r}\right]^{l+i+2} \left(\frac{2}{r_a^2}\right) w^{L(l+i+2)+1}\,dw \tag{34}$$

From (34), (12) is obtained by interchanging the order of integration and summation [49], [50]. This completes the proof.

APPENDIX G
PROOF OF COROLLARY 5

After some algebraic simplifications, (16) can be expressed as:

$$d_{f,j}^{NOMA} \approx \left(\sum_{k=0}^{K_{tr,1}} \sum_{i=0}^{k} \sum_{n=0}^{i} \sum_{l=0}^{K_{tr,2}} \sum_{q=0}^{l} \alpha(k,i,n)G(l,n,i,q)\right.$$

$$\left.\times \Xi_j(l,i)(\gamma_j^{NOMA})^{2(2+l+i)}(2+l+i)(P_r)^{-l-i}\right)$$

$$\Bigg/ \Bigg(\sum_{k=0}^{K_{tr,1}} \sum_{i=0}^{k} \sum_{n=0}^{i} \sum_{l=0}^{K_{tr,2}} \sum_{q=0}^{l} \alpha(k,i,n)G(l,n,i,q)$$

$$\times \Xi_j(l,i)(\gamma_j^{NOMA})^{2(2+l+i)}(P_r)^{-l-i}\Bigg) \tag{35}$$

Next, it is straightforward to see that:

$$\lim_{P_r \to \infty} (P_r)^{-l-i} = \begin{cases} 1, & \text{for } l = 0, i = 0 \\ 0, & \text{for } l > 0, i > 0 \end{cases} \tag{36}$$

Therefore, only $l = i = 0$ needs to be considered when evaluating $d_{f,j}^{NOMA}$ at asymptotic SNR regimes. Thus, after further algebraic simplifications, (35) reduces to $d_{f,j}^{NOMA} = 2$. This completes the proof.

REFERENCES

[1] D. W. Matolak and R. Sun, "Air-Ground Channel Characterization for Unmanned Aircraft Systems - Part III: The Suburban and Near-Urban Environments," *IEEE Trans. Veh. Technol*, vol. 66, no. 8, pp. 6607–6618, Aug. 2017.

[2] H. Hellaoui, O. Bekkouche, M. Bagaa, and T. Taleb, "Aerial Control System for Spectrum Efficiency in UAV-to-Cellular Communications," *IEEE Commun. Mag.*, vol. 56, no. 10, pp. 108–113, October 2018.

[3] Y. Liu, Z. Qin, Y. Cai, Y. Gao, G. Y. Li, and A. Nallanathan, "UAV communications based on non-orthogonal multiple access," *IEEE Wireless Commun.*, vol. 26, no. 1, pp. 52–57, 2019.

[4] Z. Yang, Z. Ding, P. Fan, and N. Al-Dhahir, "A general power allocation scheme to guarantee quality of service in downlink and uplink NOMA systems," *IEEE Trans. Wireless Commun.*, vol. 15, no. 11, pp. 7244–7257, November 2016.

[5] J.-B. Kim and I.-H. Lee, "Non-orthogonal multiple access in coordinated direct and relay transmission," *IEEE Commun. Lett.*, vol. 19, no. 11, pp. 2037–2040, November 2015.

[6] Z. Ding, P. Fan, G. K. Karagiannidis, R. Schober, and H. V. Poor, "NOMA assisted wireless caching: Strategies and performance analysis," *IEEE Trans. Commun.*, vol. 66, no. 10, pp. 4854–4876, October 2018.

[7] J. Cui, Z. Ding, and P. Fan, "A novel power allocation scheme under outage constraints in NOMA systems," *IEEE Signal Process. Lett.*, vol. 23, no. 9, pp. 1226–1230, September 2016.

[8] T. Hou, X. Sun, and Z. Song, "Outage Performance for Non-Orthogonal Multiple Access With Fixed Power Allocation Over Nakagami-m Fading Channels," *IEEE Commun. Lett.*, vol. 22, no. 4, pp. 744–747, April 2018.

[9] T. Hou, Y. Liu, Z. Song, X. Sun, and Y. Chen, "Multiple Antenna Aided NOMA in UAV Networks: A Stochastic Geometry Approach," *IEEE Trans. Commun.*, vol. 67, no. 2, pp. 1031–1044, 2018.

[10] Z. Zhang, H. Sun, and R. Q. Hu, "Downlink and uplink non-orthogonal multiple access in a dense wireless network," *IEEE J. Sel. Areas Commun.*, vol. 35, no. 12, pp. 2771–2784, December 2017.

[11] B. Xia, J. Wang, K. Xiao, Y. Gao, Y. Yao, and S. Ma, "Outage Performance Analysis for the Advanced SIC Receiver in Wireless NOMA Systems," *IEEE Trans. Veh. Technol.*, vol. 67, no. 7, pp. 6711–6715, July 2018.

[12] W. Mei and R. Zhang, "Uplink cooperative NOMA for cellular-connected UAV," *IEEE J. Sel. Topics Signal Process.*, vol. 13, no. 3, pp. 644–656, June 2019.

[13] N. Zhao, X. Pang, Z. Li, Y. Chen, F. Li, Z. Ding, and M.-S. Alouini, "Joint Trajectory and Precoding Optimization for UAV-Assisted NOMA Networks," *IEEE Trans. Commun.*, vol. 67, no. 5, pp. 3723–3735, May 2019.

[14] T. Z. H. Ernest, A. S. Madhukumar, R. P. Sirigina, and A. K. Krishna, "A Hybrid-Duplex System with Joint Detection for Interference-Limited UAV Communications," *IEEE Trans. Veh. Technol.*, vol. 68, no. 1, pp. 335–348, January 2019.

[15] ——, "A Power Series Approach for Hybrid-Duplex UAV Communication Systems under Rician Shadowed Fading," *IEEE Access*, vol. 7, pp. 76 949–76 966, June 2019.

[16] H. Jiang, Z. Zhang, L. Wu, and J. Dang, "Three-Dimensional Geometry-Based UAV-MIMO Channel Modeling for A2G Communication Environments," *IEEE Commun. Lett.*, vol. 22, no. 7, pp. 1438–1441, July 2018.

[17] T. M. Nguyen, W. Ajib, and C. Assi, "A novel cooperative NOMA for designing UAV-assisted wireless backhaul networks," *IEEE J. Sel. Areas Commun.*, vol. 36, no. 11, pp. 2497–2507, November 2018.

[18] T. Z. H. Ernest, A. S. Madhukumar, R. P. Sirigina, and A. K. Krishna, "Hybrid-Duplex Systems for UAV Communications under Rician Shadowed Fading," in *Proc. IEEE 88th Veh. Technol. Conf. (VTC Fall)*, Chicago, IL, USA, 2018, pp. 1–5.

[19] ——, "Downlink NOMA in Multi-UAV Networks over Bivariate Rician Shadowed Fading Channels," in *Proc. IEEE 90th Veh. Technol. Conf. (VTC-Fall)*, Honolulu, HI, USA, 2019.

[20] F. Jiang and A. L. Swindlehurst, "Dynamic UAV relay positioning for the ground-to-air uplink," in *2010 IEEE Globecom Workshops*. IEEE, Miami, FL, USA, 2010, pp. 1766–1770.

[21] K. Jin, X. Cheng, X. Ge, and X. Yin, "Three dimensional modeling and space-time correlation for UAV channels," in *Proc. IEEE 85th Veh. Technol. Conf. (VTC Spring)*. IEEE, Sydney, Australia, 2017, pp. 1–5.

[22] F. Jiang and A. L. Swindlehurst, "Optimization of UAV heading for the ground-to-air uplink," *IEEE J. Sel. Areas Commun.*, vol. 30, no. 5, pp. 993–1005, 2012.

[23] A. A. Khuwaja, Y. Chen, N. Zhao, M.-S. Alouini, and P. Dobbins, "A survey of channel modeling for UAV communications," *IEEE Commun. Surveys Tut.*, vol. 20, no. 4, pp. 2804–2821, 2018.

[24] N. C. Beaulieu and K. T. Hemachandra, "Novel representations for the bivariate Rician distribution," *IEEE Trans. Commun.*, vol. 59, no. 11, pp. 2951–2954, 2011.

[25] ——, "Novel simple representations for Gaussian class multivariate distributions with generalized correlation," *IEEE Trans. Inf. Theory*, vol. 57, no. 12, pp. 8072–8083, 2011.

[26] J. López-Fernández, J. F. Paris, and E. Martos-Naya, "Bivariate Rician shadowed fading model," *IEEE Trans. Veh. Technol.*, vol. 67, no. 1, pp. 378–384, 2018.

[27] P. Zhan, K. Yu, and A. L. Swindlehurst, "Wireless relay communications with unmanned aerial vehicles: Performance and optimization," *IEEE Trans. Aerosp. Electron. Syst.*, vol. 47, no. 3, pp. 2068–2085, 2011.

[28] M. Simunek, F. P. Fontan, P. Pechac, and F. J. Otero, "Space diversity gain in urban area low elevation links for surveillance applications," *IEEE Trans. Antennas Propag.*, vol. 61, no. 12, pp. 6255–6260, 2013.

[29] V. V. Chetlur and H. S. Dhillon, "Downlink coverage analysis for a finite 3-D wireless network of unmanned aerial vehicles," *IEEE Trans. Commun.*, vol. 65, no. 10, pp. 4543–4558, 2017.

[30] X. Wang, H. Zhang, Y. Tian, and V. C. Leung, "Modeling and Analysis of Aerial Base Station-Assisted Cellular Networks in Finite Areas Under LoS and NLoS Propagation," *IEEE Trans. Wireless Commun.*, vol. 17, no. 10, pp. 6985–7000, October 2018.

[31] X. Zhou, S. Durrani, J. Guo, and H. Yanikomeroglu, "Underlay drone cell for temporary events: Impact of drone height and aerial channel environments," *IEEE Internet Things J.*, 2018.

[32] P. K. Sharma and D. I. Kim, "Coverage Probability of 3-D Mobile UAV Networks," *IEEE Wireless Commun. Lett.*, vol. 8, no. 1, pp. 97–100, February 2019.

[33] T. Z. H. Ernest, A. S. Madhukumar, R. P. Sirigina, and A. K. Krishna, "Hybrid-Duplex Communications for Multi-UAV Networks: An Outage Probability Analysis," *IEEE Commun. Lett.*, vol. 23, no. 10, pp. 1831–1835, 2019.

[34] X. Liu, J. Wang, N. Zhao, Y. Chen, S. Zhang, Z. Ding, and F. R. Yu, "Placement and power allocation for NOMA-UAV networks," *IEEE Wireless Commun. Lett.*, vol. 8, no. 3, pp. 965–968, June 2019.

[35] X. Pang, G. Gui, N. Zhao, W. Zhang, Y. Chen, Z. Ding, and F. Adachi, "Uplink Precoding Optimization for NOMA Cellular-Connected UAV Networks," *IEEE Trans. Commun.*, vol. 68, no. 2, pp. 1271–1283, February 2020.

[36] R. Narasimhan, "Finite-SNR diversity–multiplexing tradeoff for correlated Rayleigh and Rician MIMO channels," *IEEE Trans. Inf. Theory*, vol. 52, no. 9, pp. 3965–3979, 2006.

[37] W.-Y. Shin, S.-Y. Chung, and Y. H. Lee, "Diversity–multiplexing tradeoff and outage performance for Rician MIMO channels," *IEEE Trans. Inf. Theory*, vol. 54, no. 3, pp. 1186–1196, 2008.

[38] T. Z. H. Ernest, A. S. Madhukumar, R. P. Sirigina, and A. K. Krishna, "Outage Analysis and Finite SNR Diversity-Multiplexing Tradeoff of Hybrid-Duplex Systems for Aeronautical Communications," *IEEE Trans. Wireless Commun.*, vol. 18, no. 4, pp. 2299–2313, March 2019.

[39] L. Zheng and D. N. C. Tse, "Diversity and multiplexing: A fundamental tradeoff in multiple-antenna channels," *IEEE Trans. Inf. Theory*, vol. 49, no. 5, pp. 1073–1096, 2003.

[40] R. U. Nabar, H. Bolcskei, and A. J. Paulraj, "Diversity and outage performance in space-time block coded Ricean MIMO channels," *IEEE Trans. Wireless Commun.*, vol. 4, no. 5, pp. 2519–2532, 2005.

[41] K. Yang, H. Cui, L. Song, and Y. Li, "Efficient full-duplex relaying with joint antenna-relay selection and self-interference suppression," *IEEE Trans. Wireless Commun.*, vol. 14, no. 7, pp. 3991–4005, 2015.

[42] A. R. Heidarpour, G. K. Kurt, and M. Uysal, "Finite-SNR Diversity-Multiplexing Tradeoff for Network Coded Cooperative OFDMA Systems," *IEEE Trans. Wireless Commun.*, vol. 16, no. 3, pp. 1385–1396, 2017.

[43] N. O'Donoughue and J. M. Moura, "On the product of independent complex gaussians," *IEEE Trans. Signal Process.*, vol. 60, no. 3, pp. 1050–1063, March 2011.

[44] R. Sun and D. W. Matolak, "Air–ground channel characterization for unmanned aircraft systems part II: Hilly and mountainous settings," *IEEE Trans. Veh. Technol.*, vol. 66, no. 3, pp. 1913–1925, March 2017.

[45] M. Alzenad, A. El-Keyi, F. Lagum, and H. Yanikomeroglu, "3-D placement of an unmanned aerial vehicle base station (UAV-BS) for energy-efficient maximal coverage," *IEEE Wireless Commun. Lett.*, vol. 6, no. 4, pp. 434–437, August 2017.

[46] M. M. Azari, F. Rosas, K.-C. Chen, and S. Pollin, "Ultra reliable uav communication using altitude and cooperation diversity," *IEEE Trans. Commun.*, vol. 66, no. 1, pp. 330–344, January 2018.

[47] T. Hou, Y. Liu, Z. Song, X. Sun, and Y. Chen, "Exploiting NOMA for UAV Communications in Large-Scale Cellular Networks," *IEEE Trans. Commun.*, vol. 67, no. 10, pp. 6897–6911, October 2019.

[48] M. Abramowitz and I. Stegun, "Handbook of mathematical functions with formulas, graphs, and mathematical tables (applied mathematics series 55)," *National Bureau of Standards, Washington, DC, USA*, 1964.

[49] I. S. Gradshteyn and I. M. Ryzhik, *Table of integrals, series, and products*. Academic press, 2014.

[50] H. Amann, J. Escher, S. Levy, and M. Cargo, *Analysis I*. Springer, Germany, 2005, vol. 3.

[51] 3GPP, "TR36.77 Study on Enhanced LTE Support for Aerial Vehicles," Tech. Rep., 2017, accessed on 23-11-2019. [Online]. Available: https://portal.3gpp.org/desktopmodules/Specifications/SpecificationDetails.aspx?specificationId=3231

[52] A. Abdi, W. C. Lau, M.-S. Alouini, and M. Kaveh, "A new simple model for land mobile satellite channels: first-and second-order statistics," *IEEE Trans. Wireless Commun.*, vol. 2, no. 3, pp. 519–528, May 2003.

[53] A. A. Nasir, H. D. Tuan, T. Q. Duong, and H. V. Poor, "UAV-enabled communication using NOMA," *IEEE Trans. Commun.*, vol. 67, no. 7, pp. 5126–5138, July 2019.

[54] H. Sallouha, M. M. Azari, A. Chiumento, and S. Pollin, "Aerial Anchors Positioning for Reliable RSS-Based Outdoor Localization in Urban Environments," *IEEE Wireless Commun. Lett.*, vol. 7, no. 3, pp. 376–379, 2017.

[55] M. Salehi, H. Tabassum, and E. Hossain, "Meta distribution of sir in large-scale uplink and downlink noma networks," *IEEE Trans. Commun.*, vol. 67, no. 4, pp. 3009–3025, April 2019.

[56] H. Tabassum, E. Hossain, and J. Hossain, "Modeling and analysis of uplink non-orthogonal multiple access in large-scale cellular networks using poisson cluster processes," *IEEE Trans. Commun.*, vol. 65, no. 8, pp. 3555–3570, August 2017.

[57] G. Geraci, M. Wildemeersch, and T. Q. Quek, "Energy efficiency of distributed signal processing in wireless networks: A cross-layer analysis," *IEEE Trans. Signal Process.*, vol. 64, no. 4, pp. 1034–1047, February 2016.

[58] C.-H. Liu and D.-C. Liang, "Heterogeneous networks with power-domain NOMA: coverage, throughput, and power allocation analysis," *IEEE Trans. Wireless Commun.*, vol. 17, no. 5, pp. 3524–3539, May 2018.

[59] M. Salehi, H. Tabassum, and E. Hossain, "Meta Distribution of SIR in Large-Scale Uplink and Downlink NOMA Networks," *IEEE Trans. Commun.*, vol. 67, no. 4, pp. 3009–3025, April 2019.

[60] S. R. Islam, N. Avazov, O. A. Dobre, and K.-S. Kwak, "Power-domain non-orthogonal multiple access (NOMA) in 5G systems: Potentials and challenges," *IEEE Commun. Surveys Tut.*, vol. 19, no. 2, pp. 721–742, 2017.

[61] A. H. A. El-Malek, F. S. Al-Qahtani, T. Q. Duong, S. A. Zummo, and H. Alnuweiri, "MIMO cognitive relay networks with correlated antennas over Rayleigh fading channels," *IEEE Trans. Veh. Technol.*, vol. 65, no. 7, pp. 5349–5363, July 2015.

[62] N. B. Rached, A. Kammoun, M.-S. Alouini, and R. Tempone, "A unified moment-based approach for the evaluation of the outage probability with noise and interference," *IEEE Trans. Wireless Commun.*, vol. 16, no. 2, pp. 1012–1023, Feb. 2017.